ISSN (Print) 1226-1750
ISSN (Online) 2233-6656
Journal of Magnetics 22(4), 531-538 (2017) https://doi.org/10.4283/JMAG.2017.22.4.531

Enhanced Detection of Defects Using GMR Sensor Based Remote Field Eddy Current Technique

J. W. Park[1], J. H. Park[1], S. J. Song[1], M. B. Kishore[1], S. G. Kwon[2], and H. J. Kim[1]*

[1]*Department of Mechanical Eng., Sungkyunkwan University, Suwon 16419, Republic of Korea*
[2]*Technology Research Department, KORAIL Research Institute, Daejeon 34618, Republic of Korea*

(Received 6 April 2017, Received in final form 26 September 2017, Accepted 29 September 2017)

Remote field eddy current testing (RFECT) can detect defects in ferromagnetic pipes without requiring a couplant and contact with the pipe wall. Because the response in the remote field zone is extremely low, testing requires high-sensitivity detection to sense low magnetic fields. Therefore, a magnetic circuit design comprising a RFECT system is necessary for excitation and reception. In this study, a RFECT system using a giant magnetoresistance (GMR) sensor is proposed, and magnetic circuits with magnets and/or yokes are designed and optimized for improved reception. To investigate the characteristics of the designed RFECT system, finite element analysis (FEA) and experiments are performed on various magnetic circuit system configurations. System performance is verified with respect to sensitivity and the detectability of defect characterizations in 4-inch ferromagnetic pipelines having different defect sizes. Consequently, the magnetic circuit system using the permalloy yoke shows the highest sensitivity, thus achieving effective RFECT detection.

Keywords : remote field eddy current testing (RFECT), giant magnetoresistance (GMR) sensor, ferromagnetic pipe, magnetic circuit system, nondestructive testing

1. Introduction

Pipelines and pipeline facilities are among the most important elements in industrial facilities and have broad applications in the energy industry. However, leakage or rupture of the pipelines in petrochemical facilities, city gas supplies, etc., can lead to fires and large explosions, resulting in harm to the economy and human life. nondestructive evaluation (NDE) methods are handy tools for detecting and evaluating various kinds of defects associated with pipelines. A wide range of NDE methods, including ultrasonic testing (UT), radiography testing (RT), and magnetic flux leakage (MFL), are used for pipeline inspection [1]. The remote field eddy current testing (RFECT) technique has attracted the attention of researchers recently, owing to its equal sensitivity detection for inner and outer defects [2], and it has been applied extensively to oil storage and gas pipeline inspections [3-6].

The design of the receiving sensor used in RFECT is different from that used in conventional eddy current testing (ECT); RFECT is a method in which a receiving sensor receives a magnetic field generated from an exciter sensor inside a pipeline to obtain information about the pipeline [7]. The RFECT technique has advantages over other eddy current techniques; however, like all other methods, the signal to noise ratio (SNR) and defect detection ability of the technique fundamentally depend on the performance of the sensors. The solenoid coil, which is a conventional receiving sensor, showed low SNR in the pipeline [5]. In addition, when an array system is constructed for the inspection of an entire pipeline, a difference in coil impedance among the receiving sensors directly affects the defect detection ability [8]. Moreover, it is difficult to replace these sensors when they are damaged and to construct an array system for smaller diameter pipelines, because of sensor size limitation [8]. To solve this problem, magnetoresistance (MR) sensors, high-precision amplifiers, advanced signal processing techniques, and other filtering techniques to eliminate external noise were introduced [9, 10]. In particular, among the MR sensors, the giant magnetoresistance (GMR) sensor is small, low cost, and has high sensitivity. A characteristic of the GMR sensor is that the output value

*Corresponding author: Tel: +82-31-290-7460
Fax: +82-31-290-5889, e-mail: hjkim21c@skku.edu

changes based on the hysteresis curve, according to the intensity change of the external magnetic field [8]. However, because the magnitude of the defect signal obtained by the GMR sensor is small, signal enhancement is needed. Previous studies reported on the use of permanent magnets to enhance the signal of the GMR sensor. In these research papers, the authors compared anisotropic magnetoresistance (AMR) and the GMR sensor, and concluded that GMR sensors are the best suited for defect detection with some simulation result except for experimental evidence [11, 12].

In this study, the GMR sensor was applied to the receiving sensor of the RFECT, instead of the conventional solenoid coil, to investigate the direction in which the GMR sensor has better sensitivity by comparing the characteristics of the defect signal in axial and radial directions. However, because the acquired signal was small in magnitude, signal enhancement was needed. Based on the simulation results of the signal-enhancement factor, a stand-alone GMR sensor and GMR sensors with two different designs were designed and evaluated by experiment. Additionally, after selecting the best sensor for signal enhancement, an experiment was conducted to confirm the maximum lift-off distance between the sensor and pipe wall by increasing the lift-off distance.

2. Design Configuration of the GMR Sensor for Signal Enhancement

2.1. Simulation of signal enhancement factors

Numerical simulations were carried out for comparison of the signal-enhancing factors of the GMR sensor using COMSOL commercial software package. The receiving sensor (GMR sensor) was assumed, and was placed at an arbitrary position because it was difficult to implement in simulations. The sensing direction of the GMR sensor was set to the axial direction. Neodymium and permalloy were used for the material properties of the permanent magnet and yoke, respectively, and carbon steel was used for the pipe. The size of the magnets was 3 mm in width and 3 mm in length, and the permalloy yoke was 4.5 mm in width and 5 mm in length. For the GMR sensor with magnet simulation, ‘magnetic field’ and ‘magnetic and electric fields’ studies were applied, and permeability of the permalloy was set to 8000. The exciter sensor had a wire diameter of 0.75 mm, winding of 2000 turns, and the exciting current was 1 A with a frequency of 40 Hz.

Figure 1 shows the magnetic field vector of the stand-alone GMR sensor and the GMR sensors with two different designs when an arbitrary defect was located under the center of the sensor. Figure 1(a) shows directional distribution of the magnetic field vector for a stand-alone GMR sensor. It can be observed that the direction of the magnetic field vectors is in the axial direction of the pipe, at the internal part of the pipe, because the GMR sensor does not affect the remote magnetic field generated from the exciter sensor. As shown in Fig. 1(b), when a magnet is attached to the GMR sensor, a phenomenon of attracting an external magnetic field occurs. Owing to the magnetic field generated by the magnet, concentration of the magnetic field on the flux concentrator (a GMR element covered by a permalloy material) is increased and affects the signal enhancement of the sensor. The direction of the magnetic field vector is changed from the axial to the radial direction, because of the effect of the magnet. Therefore, when the magnet is attached to the GMR sensor, the radial direction field, instead of the axial direction field, substantially affects the sensor. However, signal enhancement is determined by the location of the magnet. The signal was enhanced when the magnet was attached to the upper side of the GMR sensor, but there was no effect when it was attached to the lateral face. Permalloys are magnetic materials with high permeability and are used for devices requiring magnetic amplification. Fig. 1(c) shows a GMR sensor with yoke; as shown in the figure, an external magnetic field is concentrated on the

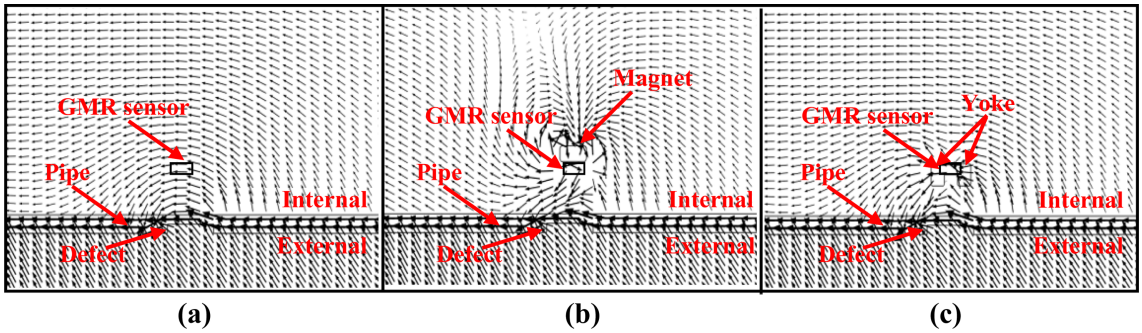

Fig. 1. (Color online) Simulation of factors affecting the signal enhancement of the GMR sensor: (a) Stand-alone GMR sensor, (b) GMR sensor with magnet, and (c) GMR sensor with yoke.

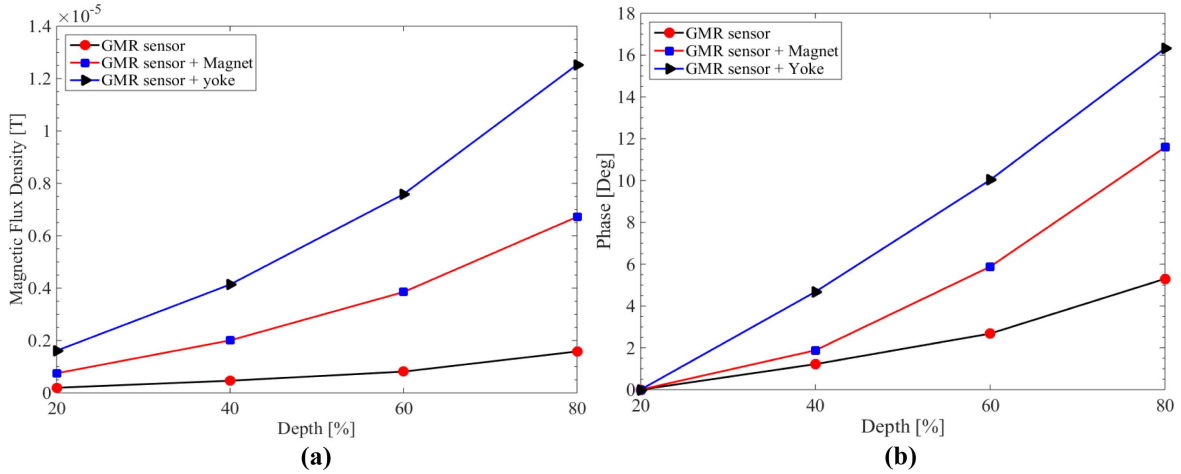

Fig. 2. (Color online) Defect signals of depth from 20 % to 80 % obtained in simulation of the stand-alone GMR sensor and the GMR sensors with two different designs: (a) Amplitude and (b) Phase.

yoke and transmitted to the GMR sensor. This configuration utilizes the characteristics of the GMR sensor, whose sensitivity varies with the intensity of the external magnetic field. For example, two flux concentrators are configured on both ends of a GMR sensor and this element transmits a concentrated magnetic field to a sensing element. The flux concentrator shows increased sensitivity as its size is increased and the distance between the two concentrators decreases [13]. Using the same principle, the magnetic field concentrated on the yoke is transferred to the GMR sensor and affects signal enhancement.

Figure 2 shows the amplitude and phase values of the defect signals from the stand-alone GMR sensor and the GMR sensors with two different designs for the defects with depths from 20 to 80 % of the specimen thickness. As shown in Fig. 2(a), the result obtained with the GMR sensor with yoke shows the amplitude of the signal compared to the other two sensors. As shown in Fig. 2(b), the signal is compared by normalizing the phase change of the stand-alone GMR sensor and the GMR sensors with two different designs for the defects. The phase change of the GMR sensor with yoke was the largest. Therefore, it was confirmed that the GMR sensor with yoke had the best signal enhancement among the stand-alone GMR sensor and the GMR sensors with two different designs.

2.2. Experimental Setup

A function generator (Tektronix) was used to generate a 40 Hz sine wave, which was amplified by a bipolar amplifier (Kepco) to operate the exciter sensor. The defect signal measured by the GMR sensor (NVE AA002-02) was filtered and amplified using a lock-in amplifier (Stanford). The signal (X: In-phase, Y: Quadrature) was obtained by the auto scanning system, with real time monitoring and signal storage in the acquisition program via the data acquisition (DAQ) [8].

As shown in Fig. 3, the sensors used for this experiment consist of an exciter sensor and a GMR sensor. The GMR sensor had two different directional arrangements: the axial and radial directions of the pipe. The design of the exciter sensor was ϕ100 mm outer diameter, ϕ26.33 mm inner diameter, ϕ0.75 mm wire diameter, and 2000 turns. The stand-alone GMR sensor and the GMR sensors with two different designs were designed based on the results of the simulation. The first configuration is a stand-alone GMR sensor, and the second is a GMR sensor with a permanent magnet suitable for the experiment. The magnet was placed on the bottom surface of the GMR sensor

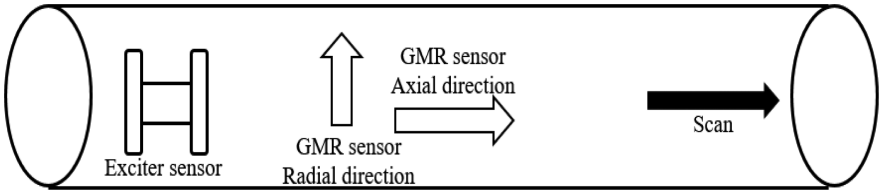

Fig. 3. Schematic of the GMR sensor based RFECT.

Table 1. Depth specifications of flat-bottom hole defects.

% of wall loss	20 %	40 %	60 %	80 %
Defect depth	0.9 mm	1.8 mm	2.7 mm	3.6 mm

based on the simulation results. Finally, the third configuration uses a permalloy yoke attached to the sensor jig. The radial direction was placed at the upper part of the sensor to eliminate common difficulties owing to lift-off effects. An auto scanning system was designed and manufactured for the exciter and GMR sensor to enable scanning with constant speed, and an encoder was connected to it so that the scanning distance could be accurately measured. The RFECT signal was measured by scanning 400 mm, and the defect signal was measured by scanning 500 mm. In addition, to avoid the edge effect, the experiment was conducted on an area twice the pipe diameter apart from both ends of the pipe. The lift-off distance of the GMR sensor was controlled by applying an LM guide on the GMR sensor module to increase the distance with a 5 mm step.

For the specimen, four flat-bottom hole (FBH) type defects, each having a 9 mm diameter occurring at regular intervals of 100 mm on the outer surface, was machined on a 1000 mm long 4-inch ferromagnetic pipe having a 105.3 mm inner diameter and 114.3 mm outer diameter. Table 1 gives the depth specifications of the respective defects.

3. Experiment Results and Discussion

The results of the axial and radial direction testing of the GMR sensor were compared to determine the best detection method. Based on the obtained results, the stand-alone GMR sensor and the GMR sensors with two different designs were configured and compared for evaluation. Preliminary experiments were conducted to select the appropriate position of the GMR sensor in the remote magnetic field zone. This measurement is necessary to determine the optimum distance between the exciter and GMR sensor.

3.1. RFECT signals of axial and radial directions

To determine the distance between the GMR sensor and exciter coil, experiments were conducted by slowly moving the GMR sensor away from the exciter sensor in the non-defect pipe. Figure 4 shows the RFECT signals acquired from the GMR sensor in the axial and radial directions; the distances at which the remote magnetic field starts to appear were different. The transition zone was clearly observed as shown in Fig. 4. The transition

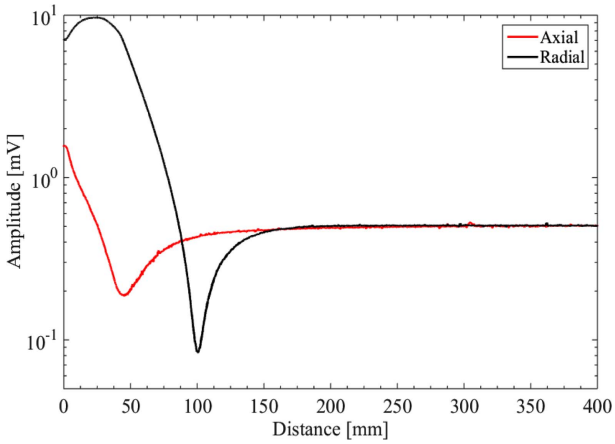

Fig. 4. (Color online) RFECT signals of the GMR sensor in axial and radial directions.

zone can be clearly identified by the phase reversal, although the magnetic flux density at potential energy is theoretically zero. In the direct field zone, the magnetic flux density rapidly decreased and gradually increased before it became constant in the remote field zone. Therefore, it was observed that the distance of the GMR sensor from the exciter sensor should be 120 mm in the axial direction, and 180 mm in the radial direction. Further increase of the distance between the exciter and the GMR sensor in the remote field zone did not cause attenuation of the RFECT signal in either the axial or radial direction. In addition, the magnitude of the signals in the radial direction was approximately 0.05 mV larger than that in the axial direction. Therefore, the distance between the GMR sensor and the exciter sensor was determined to be 180 mm based on the remote magnetic field zone of the radial direction case.

3.2. Defect signal characteristics in axial and radial directions

Figure 5 shows the in-phase and quadrature components of the defect signals measured by the GMR sensor in the axial and radial directions. The defect signals in the figure were obtained from the defect having a depth of 80 %. As shown, the in-phase and quadrature components are different depending on the direction of the magnetic field leakage from the defect. When the signals of Fig. 5(a) and (b) are compared, the in-phase component shows a larger signal than the quadrature component. Thus, the in-phase component affects the signal more than the quadrature component. Additionally, as shown in Fig. 5(a), it is advantageous to arrange the GMR sensor in the radial direction because the GMR sensor shows a larger signal than in the axial direction.

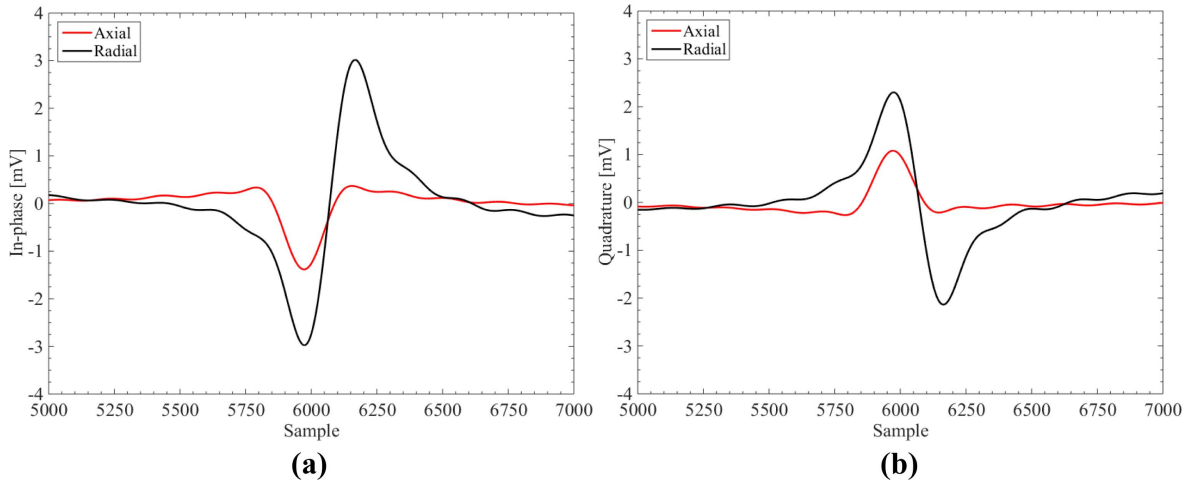

Fig. 5. (Color online) In-phase and quadrature components of the defect signals measured by the GMR sensor in axial and radial directions: (a) In-phase and (b) Quadrature.

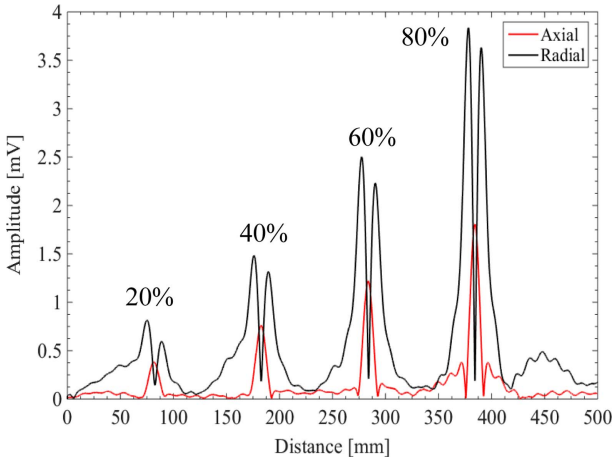

Fig. 6. (Color online) RFECT signals acquired from scanning the GMR sensor in axial and radial direction configurations.

As shown in Fig. 6, when the defect signals having defect depths from 20 % to 80 % were compared, the amplitude of the defect signals increased linearly with increasing depth of defects in both the axial and radial direction cases. In addition, for each defect, the signal of the radial direction is about two times larger than that of the axial direction. In the radial direction case, the defect signal shows two peaks at each defect; whereas, the axial direction shows only one peak perfectly aligned midway between the two peaks that resulted from the radial direction. This phenomenon can be explained in terms of sensor dimensions and defect diameter. Because the defects are separated by a distance of 100 mm, the peaks obtained from the GMR sensor exactly correspond to the defect position and the width of the detected signal is approximately 9 mm, which is the diameter of the defect. In the axial direction case, the face of the GMR sensor approximately covers the 9 mm defect surface; however, in the radial direction case, the 1.3 mm thickness of the sensor cannot cover the entire defect surface. Because of this, the signal has two peaks between each change in pipe thickness. The first peak is higher than the second peak because the first peak occurred when the sensor moved from the non-defect part of the pipeline to the defect part. Therefore, it can be concluded that the GMR sensor in the radial direction can improve the sensitivity from these features of the signal and estimate the defect.

3.3. Comparison of defect signals for evaluation of stand-alone GMR sensor and the GMR sensors with two different designs for signal enhancement

Based on the comparison results of the defect signals in the axial and radial directions, the defect signals of the stand-alone GMR sensor and the GMR sensors with two different designs in the radial direction were compared. Figure 7(a) shows the amplitude of the signal measured by the stand-alone GMR sensor and the GMR sensors with two different designs. As the depth of the defect increases, the amplitude of the signal increases linearly. The GMR sensor with yoke showed the largest signal amplitude and the stand-alone GMR sensor showed the smallest. Based on a defect depth of 80 %, the signal enhancement was approximately 38 %. Fig. 7(b) is a Lissajous pattern of the defect signal obtained in the GMR sensor with yoke case, having a defect depth of 20 % to 80 %. These patterns are useful for calculating the phase change of the defect signal. As the defect depth increased from 20 % to 80 %, the Lissajous pattern rotated counterclockwise and the radius of curvature was increas-

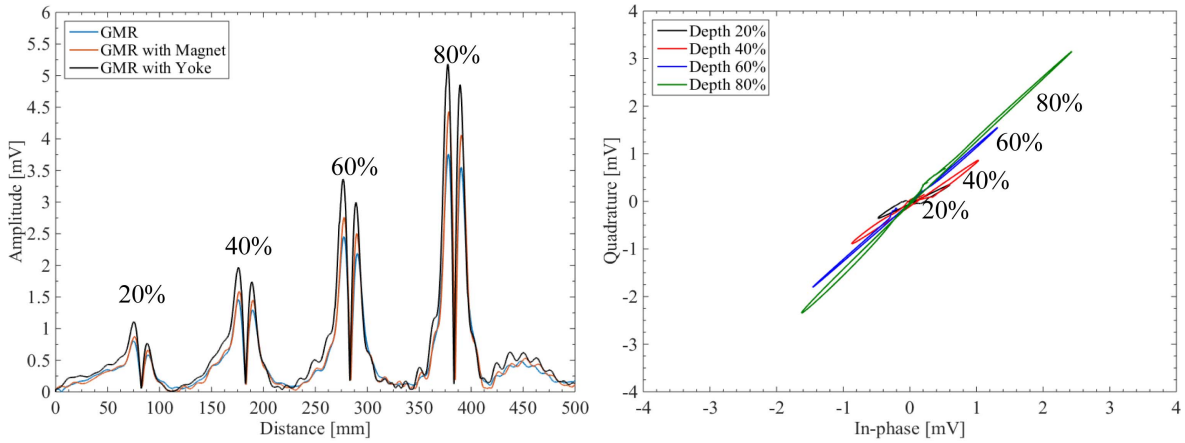

Fig. 7. (Color online) (a) Amplitude of the defect signals obtained using the stand-alone GMR sensor and the GMR sensors with two different designs in the radial direction, and (b) the Lissajous pattern of defect signal of the GMR sensor with yoke.

ed; thus, the phase value increased.

Figure 8(a) shows the amplitudes of the defect signal corresponding to the four defects with depth varying from 20 % to 80 %. It was already proved that as the defect depth increased from 20 % to 80 %, the amplitude value linearly increased. Therefore, as shown in Fig. 8(a), the value of the amplitude increases as the defect depth increases. In the GMR sensor with magnet case, the sensitivity was increased by 45 % compared to the stand-alone GMR sensor.

When a permalloy yoke was attached to the GMR sensor, the signal level was further increased compared to both of the previous cases and the sensitivity was increased by 80 % compared to the stand-alone GMR sensor. It was expected that the yoke would concentrate the magnetic field on the sensor, thereby increasing the signal level. In conclusion, as shown in Fig. 8, the permalloy yoke shows the best performance among the stand-alone GMR sensor and the GMR sensors with two different designs. This result is attributed to the basic property of permalloy with high permeability to concentrate the magnetic field in the GMR element. Figure 8(b) shows the phase values calculated from the Lissajous patterns of the defect signal measured by the stand-alone GMR sensor and the GMR sensors with two different designs. As the depth of the defect is increasing, the phase value is also increasing. The phase change is also similar to the amplitude change, and using the permalloy yoke gives maximum phase change of the defect signal at a defect depth between 20 % and 80 %. In the radial direction case, the maximum phase change is about 30 °. The GMR sensor with yoke shows enhanced detection of defects in both amplitude

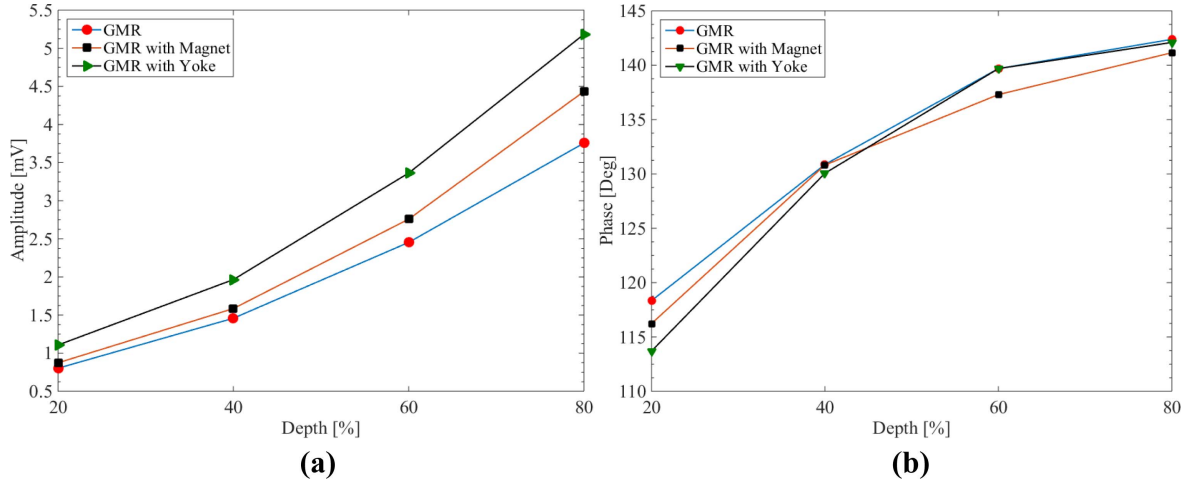

Fig. 8. (Color online) Amplitude and phase of the defect signals of the stand-alone GMR sensor and the GMR sensors with two different designs with increasing depth of the defect: (a) Amplitude and (b) Phase.

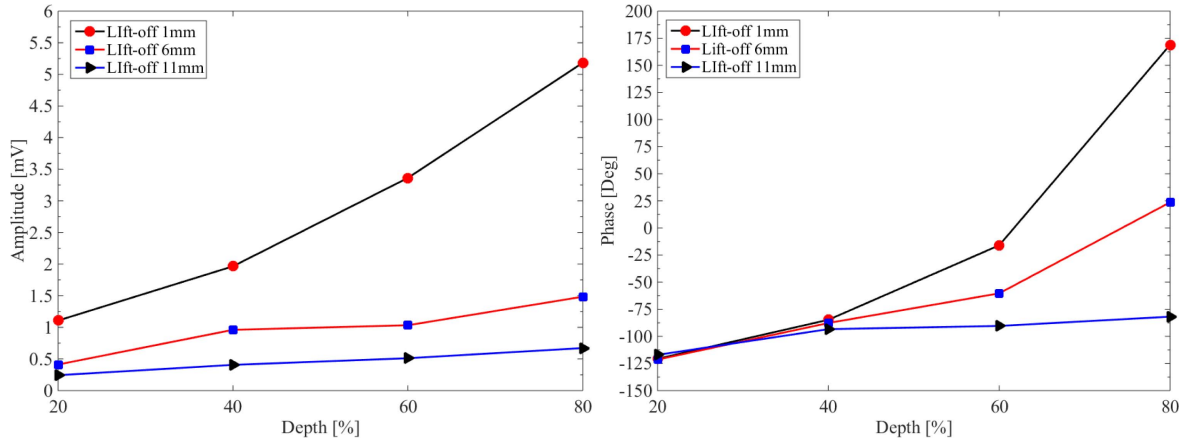

Fig. 9. (Color online) Amplitude and phase of the defect signals with increasing lift-off: (a) Amplitude and (b) Phase.

and phase.

3.4. Comparative evaluation of different lift-off distances in the GMR sensor with yoke case

The GMR sensor with yoke, which showed the largest defect signal among the stand-alone GMR sensor and the GMR sensors with two different designs, was used to compare the effects of increasing lift-off. The lift-off was increased from 1 mm to 11 mm, and the amplitude and phase of the defect signals resulting from the experiment are shown in Fig 9. As the lift-off increases, the amplitude and phase of the defect signals for each defect decrease. It was expected that the sensor would detect the defects until the 6 mm lift-off. However, until the 11 mm lift-off, a considerable change which can discriminate the defects can be observed, although the sensitivity is poor. As shown in Fig. 8(a), the amplitude of the defect signals changes significantly as the lift-off increases. However, in the phase case shown in Fig. 9(b), the change of the signal from the 60 % defect was large. Until the 11 mm lift-off, detection of the defect having depths from 20 % to 80 % was possible.

4. Conclusion

In this study, we compared and evaluated the factors affecting the signal enhancement of the GMR sensor using the RFECT method in a 4-inch ferromagnetic pipeline. First, the distance between the exciter sensor and GMR sensor was determined to be about 180 mm. After comparing the defects signals in the axial and radial directions of the GMR sensor with the determined distance, we acquired the result that the defect signal is larger when the GMR sensor is arranged in a radial direction, compared to the case when it is in an axial direction. Based on the simulation results, a ferromagnetic pipe having a wall thickness of 4.5 mm, with a 9 mm diameter FBH type defect having a depth ranging from 20 % to 80 % of the wall thickness on the outer surface, was tested using the designed stand-alone GMR sensor and the GMR sensors with two different designs. Results from comparing the defect signals of the stand-alone GMR sensor and the GMR sensors with two different designs indicate that the GMR sensor with yoke arranged in the radial direction showed the best detection ability for both the amplitude and phase signals. The performance of the GMR sensor with yoke was increased by 80 % compared to the stand-alone GMR sensor.

Acknowledgements

This research was carried out with the support of the project development of rail-damage detection inspection and monitoring system for advanced prevention railway obstruction among the railroad technology research projects supported by the Korea Agency for Infrastructure Technology Advancement (KAIA).

References

[1] Albert Teitsma, Stephen Takach, Julie Maupin, Jennifer Fox, Paul Shuttleworth, and Paul Seger, J. Pressure Vessel Technol. **127**, 269 (2005).
[2] Hagen Schempf, Edward Mutschler, Alan Gavaert, George Skoptsov, and William Crowley, J. Field Robot, **27**, 217 (2010).
[3] Gopal Gantala, C. V. Krishnamurthy, and Krishnan Balasubramaniam, J. Nondestruct. Eval. **35**, 2 (2016).
[4] Y. B. Chen, J. Zheng, and W. J. Luo, ASME Press. Vess.

Pip. **5**, 237 (2012).
[5] X. J. Xu, M. Liu, Z. B. Zhang, and Y. L. Jia, Sensors **14**, 24098 (2014).
[6] K. L. Yu, M. K. Hui, and S. P. Gwan, J. Korean Magn. Soc. **24**, 171 (2014).
[7] Xiaojie Xu, Ming Liu, Zhanbin Zhang, and Yueling Jia, Sensor. **14**, (2014) 24098.
[8] J. W. Park, J. H. Park, S. H. Song, H. J. Kim, and S. G. Kwon, KSNT **36**, 483 (2016).
[9] Y.-J. Kim and S.-S. Lee, NDT&E International. **49**, 77 (2012).
[10] Junjun Xin, Naiguang Lei, Lalita Udpa, and Satish Udpa, IEEE Trans. Magn. **47**, 1070 (2011).
[11] Dario J. L. Pasadas, A. Lopes Ribeiro, Helena G. Ramos, and Tiago J. Rocha, Acta IMEKO, **4**, 62 (2015).
[12] Dario J. Pasadas, Tiago J. Rocha, Helena G. Ramos, and A. Lopes Ribeiro, Instrumentation and Measurement Technology Conference (IMTC) (2013) pp 296-299.
[13] K. Y. Kim and Y. J. Oh, Ceramist **4**, 44 (2001).